water

MDPI

Article

Shear Strength of Loess in the Yili Region and Corresponding Degradation Mechanisms under Different Cycling Modes

Yongliang Zhang [1], Zizhao Zhang [1,2,*], Wanhong Hu [1], Yanyang Zhang [1,*], Guangming Shi [1] and Yamei Wang [1]

[1] School of Geological and Mining Engineering, Xinjiang University, Urumqi 830017, China; zyl15193288192@163.com (Y.Z.); 13330383003@163.com (W.H.); shiguangming@xju.edu.cn (G.S.); ym19863815195@163.com (Y.W.)

[2] State Key Laboratory for Geomechanics and Deep Underground Engineering, Xinjiang University, Urumqi 830017, China

* Correspondence: zhangzizhao@xju.edu.cn (Z.Z.); zyy@xju.edu.cn (Y.Z.); Tel.: +86-136-3997-7295 (Z.Z.); +86-132-0138-6511 (Y.Z.)

Abstract: In the Yili region, China, complex environmental conditions induce repeated wet–dry (WD) and freeze–thaw (FT) cycles, deteriorating soil shear strength and producing frequent loess landslides. In this study, we collected soil samples from the Alemale landslide, Yili Prefecture and performed their triaxial shear tests with different numbers of WD, FT, and WD-FT cycles. In addition, we summarized the change mechanisms of loess mechanical properties and its deterioration, in the Yili region, under different cyclic effects. Subsequently, the test results under the three cycling modes were compared and analyzed, the differences in the deterioration effects of different cyclic conditions on loess were discussed in depth, and finally, a multiple linear regression model was established and the weights of single factors under the action of coupled cycles were analyzed. The results show the following: (1) Regardless of the confining pressure values, the principal stress evolution trends in soil samples under different cycling modes were generally consistent, i.e., after an initial increase, peak values were reached, followed by a final decline. (2) Under unconsolidated undrained (UU) conditions, shear strength values of all soil samples tested under the three cycling modes dropped after the first twenty cycles, exhibiting different evolution patterns. (3) Coupled WD-FT cycling most significantly promoted soil shear strength degradation, with less WD cycling effect, and FT cycling had the least significant effect; in all three modes, the first cycle had the highest contribution to this effect. From the perspectives of cohesion, angle of internal friction, and decay of shear strength attenuation, the coupled WD-FT cycling effect on soil shear strength could not be reduced to a simple single-factor addition–subtraction relationship. (4) Weight analysis of soil samples after WD, FT, and WD-FT cycling revealed that WD cycles in the coupled WD-FT cycling mode had the most significant impact on the shear strength attenuation of soil samples (contributing 57%), FT cycles had a medium impact (contributing about 33%), while the effect of the total number of cycles was negligible (about 10%). The research results provide experimental and theoretical bases for subsequent control of loess landslides.

Keywords: Yili loess; wet–dry cycles; freeze–thaw cycles; soil shear strength attenuation; internal friction angle; cohesion

Citation: Zhang, Y.; Zhang, Z.; Hu, W.; Zhang, Y.; Shi, G.; Wang, Y. Shear Strength of Loess in the Yili Region and Corresponding Degradation Mechanisms under Different Cycling Modes. *Water* **2023**, *15*, 3382. https://doi.org/10.3390/w15193382

Academic Editor: Yeshuang Xu

Received: 11 August 2023
Revised: 11 September 2023
Accepted: 16 September 2023
Published: 27 September 2023

1. Introduction

The Yili region of China is famous worldwide for its loess soil, which is widely distributed and has a thick, loose structure [1]. Due to seasonal and periodic changes in temperature and precipitation, the loess experiences repeated freezing, melting, water absorption, and dehydration long-term processes [2,3], implying soil strength deterioration under multiple WD and FT cycles [4–8]. Heavy rainfalls can lead to deformation and strength degradation of soil, which is the main cause of slope instability in loess. WD

cycling has also been shown to significantly deteriorate the mechanical properties and microstructure of loess, leading to loess sliding failure [9,10]. FT cycling is a specific form of temperature variation that involves ice crystal formation and melting which change the alignment of soil grains and complicate the variation pattern of the soil mechanical properties [11–13]. Under coupled WD-FT cycling, aggregates in soil undergo repeated splitting and agglomeration. After breaking the coupling force of soil particles, the particles sink under the action of gravity. After rearranging, the soil pores grow and the size and spacing among soil particles become more uniform [14–16]. The evolution trends of loess mechanical properties under different cycling modes have been investigated from different perspectives.

(1) Loess after WD cycling: Jiang et al. [17] studied the landslide slip zone soil of a specific accumulation layer in the Three Gorges Reservoir area and found that as the number of WD cycles increased, the air intake valve and residual water level of the soil declined gradually, and the WD cycles weakening of the soil cohesion was greater than that of the angle of internal friction. Pan et al. [18] tested WD cycles on loess in the Yan'an area and concluded that with an increase in the the number of WD cycles and moisture content, cementation between soil particles decreased, and the shear strength, cohesion, and the angle of internal friction values decreased. Chang et al. [19] conducted four groups of tests on saturated permeability and soil-water characteristics under different WD cycling paths; they reported that the relationship between the degradation degree of the original loess saturated permeability coefficient and the number of WD cycles could be depicted by a hyperbolic function. After six cycles, the change in deterioration degree tended to be stable. Hao et al. [20] performed laboratory tests and revealed that WD cycling caused soil structure damage, deteriorating the soil strength and deformation characteristics.

(2) Loess after FT cycling: Xie et al. [21] conducted FT cycling tests on primary and remodeled loess samples from the Xining region, Qinghai, China, and reported that the compressive strength of unperturbed loess was greater than that of remodeled loess; meanwhile, with an increase in the number of FT cycles, the large particles of loess gradually decomposed into small particles, and the arrangement of particles was changed. Additionally, the direct shear experiment of expansive soil after FT cycling revealed that FT cycles decreased the soil samples' elastic modulus and cohesion and increased the internal friction angle [22–24]. Through indoor experiments, Lv et al. [25] clarified the FT cycling-induced soil structural changes.

(3) Loess under coupled WD-FT cycling: Zhang [26] reported that the compression modulus of reshaped loess decreased significantly with the number of coupled WD-FT cycles. Rui et al. [27] investigated, in detail, the impact of WD-FT cycling on the physical behavior of exfiltrated soils, and reported its important impact on the attenuation of the mechanical properties of expansive soils, resulting in reductions in the elastic modulus, breaking strength, adhesion, and the angle of internal friction; a normalized stress–strain relationship was also proposed to take into consideration the WD-FT cycling and the enclosing pressure. Yang et al. [28] carried out dynamic triaxial tests with coupled WD-FT cycling for alkali slag-solidified light soil. The results showed that as the number of coupled WD-FT cycles increased, the axial strain of the solidified soil increased and the freezing temperature decreased; the impact of the first three cycles was relatively large, and it reached stability after the fifth cycle.

Although the available methods for studying the macroscopic properties of soil are relatively mature, most studies have concentrated on variations in soil mechanical properties under the influence of a singular factor. However, many factors simultaneously affect the shear strength of soil, and their respective contributions and coupling still have to be clarified to comprehensively reflect the evolution laws of loess strength characteristics. Hence, it is essential to experimentally identify the adjustments in the physical mechanisms of loess, in the Yili region, under different cycling modes and to theoretically substantiate them.

To this end, the current study took a typical loess landslide, i.e., the Alemale landslide slippery soil in the Yili region, China, as the research object. Considering the periodic change conditions of the local climate, test programs for WD, FT, and coupled WD-FT cycling were designed and realized. Through comprehensive research on the trends of soil shear strength degradation, we applied the available strength and deformation theories to establish the change mechanisms of the loess mechanical properties, in the Yili region, under WD, FT, and couple WD-FT cycling modes and different numbers of cycles. The results obtained are expected to lay a solid theoretical foundation for future landslide control in this and similar loess areas.

2. Experimental

2.1. Determination of Basic Physical Indicators

The loess required for the soil samples was collected from the west side of the Hain Desayi Valley near Alemale Town, Xinyuan County, in the Yili region (Figure 1). The sampling depth was 2 m, and the total sample weight was approximately 30 kg. After the on-site sampling was completed, indoor test analysis was carried out, and the natural water content, natural density, max. dry density, and saturated water capacity of loess in the Yili region were calculated. The natural moisture content of the samples was 20.5%, the natural density was 1.95 g/cm^3, the maximum dry density was 1.86 g/cm^3, and the saturated water content was 24.3%, as obtained by experimental calculations.

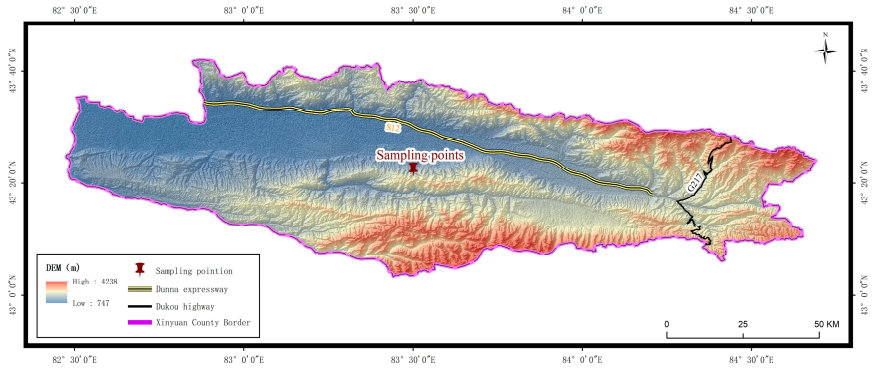

Figure 1. Map of sampling locations in the study area (figure DEM data from geospatial data in the Cloud).

2.2. Experimental Procedures

2.2.1. Preparation of Soil Samples

According to the geotechnical test method standard, we spread the block disturbed soil in a cool place for air drying. Then, the air-dried soil was pulverized with a pulverizer and sieved using a 2 mm sieve (Figure 2a). Then, the spray method was used to prepare the remodeling samples according to the natural water content of 20.5%. First, the estimated amount of water was sprayed using the spray equipment; the samples were fully stirred, put into containers, sealed, and put it in a shady location to moisten for a night and a day for later use. Finally, we used the compaction method to prepare remolded samples according to the maximum dry density of 1.86 g/cm^3 (Figure 2b).

2.2.2. WD Cycling Tests

We soaked the soil samples and dried them in an oven to simulate rainfall and evaporation experienced by soil under actual conditions. The water contents in the dry state and after humidification were 20.5 and 24.3%, respectively. After the soil samples were humidified, they were placed in a moisturizing dish and allowed to stand for 24 h to achieve even water distribution. The water content control of the circulating soil samples is shown in Figure 3. When the soil samples underwent the humidification–dehumidification (WD) process and reached the preset water content, the end of the WD cycling test was

marked. The numbers of cycles for the WD cycling test set in the experiment were 0, 1, 5, 10, 15, and 20 cycles.

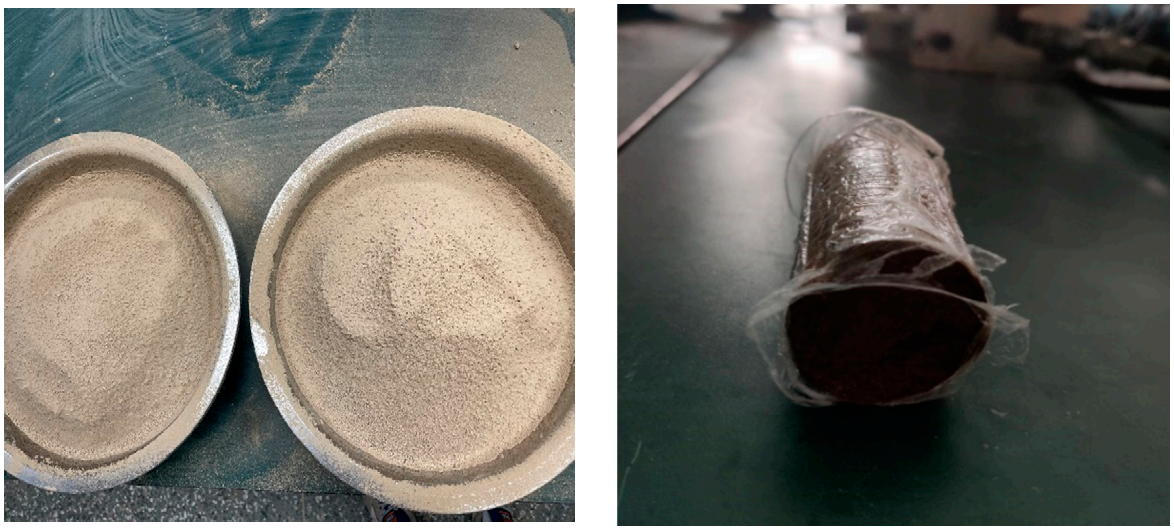

(**a**) (**b**)

Figure 2. Procedure for preparing test soil samples (**a**) Crushed and sieved soil; (**b**) Partially fabricated specimen.

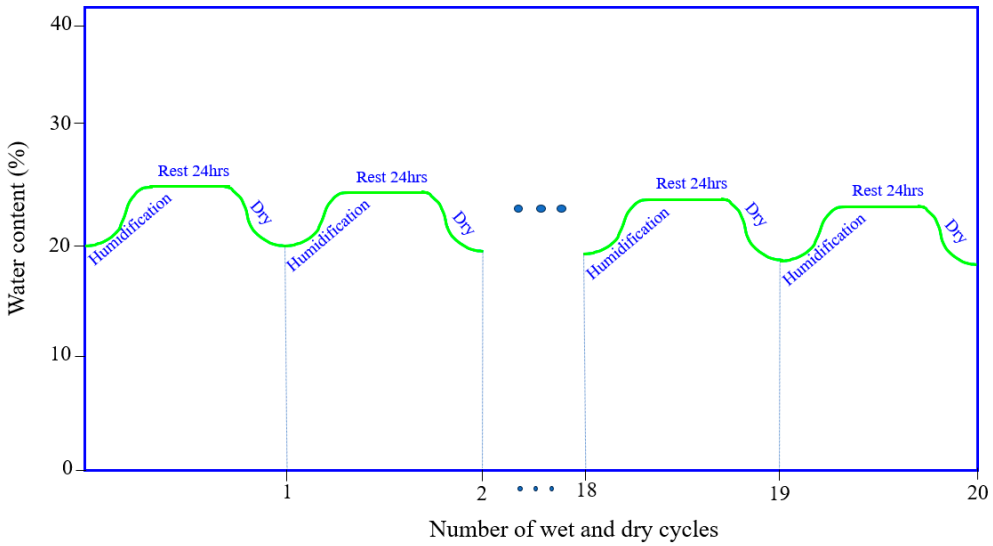

Figure 3. Schematic diagram of wet–dry cycling.

2.2.3. FT Cycling Tests

We placed the soil samples in a JW-2000 series constant temperature and humidity test chamber to simulate freezing and melting effects experienced by soil under actual conditions. According to the local meteorological circumstances, the freezing temperature of the FT cycle was set at −15 °C for 15 h, with ablation at 15 °C for 9 h. The temperature control of the cyclic specimen is shown in Figure 4. The numbers of cycles for the FT cycling tests were 0, 1, 5, 10, 15, and 20 cycles.

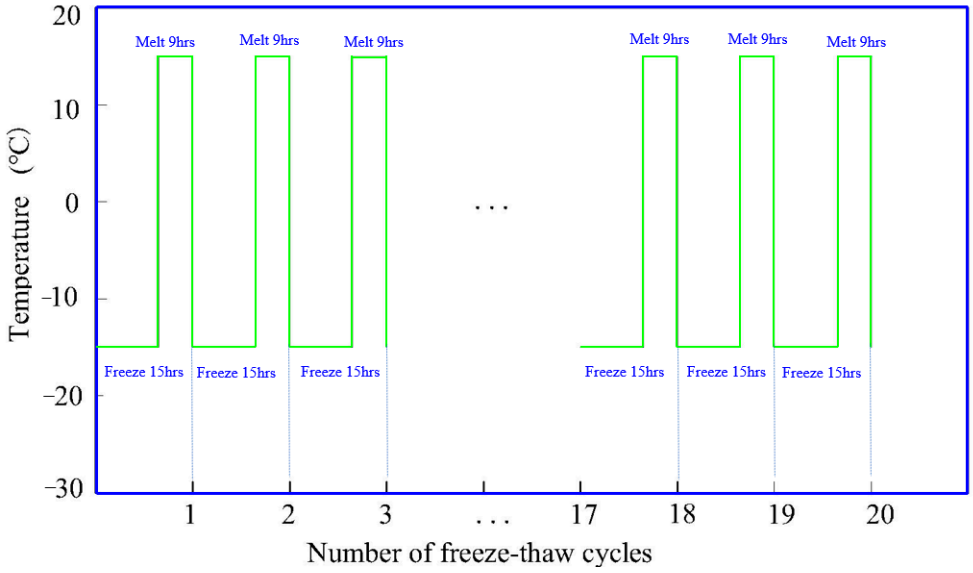

Figure 4. Schematic diagram of freeze–thaw cycling.

2.2.4. Coupled WD-FT Cycling Tests

We soaked and humidified the soil samples, and dried them in an oven, to simulate rainfall, evaporation, freezing, and ablation cycles experienced by soil under actual conditions. After the soil samples were humidified, we placed them in a moisturizing dish and allowed them to stand for 24 h to achieve even water distribution. Then, we immediately placed the samples into the above-mentioned JW-2000 series chamber for the FT cycling test. According to the local meteorological environment, the freezing temperature of the FT cycle was set at −15 °C for 15 h, with ablation at 15 °C for 9 h (Figure 5). The numbers of cycles for the coupled WD-FT cycling tests were 0, 1, 5, 10, 15 and 20 cycles.

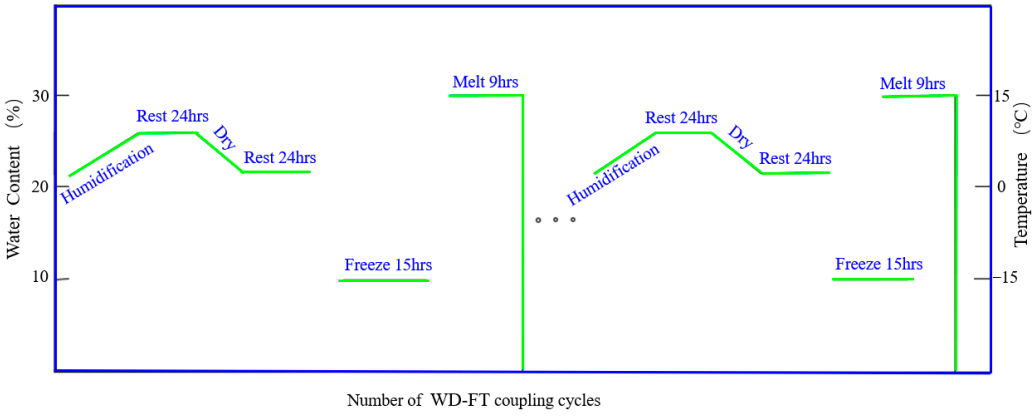

Figure 5. Schematic diagram of coupled WD-FT cycling.

2.2.5. Triaxial Shear Tests

We subjected the soil samples to triaxial shear tests based on a TFB-1 unsaturated soil stress and strain control triaxial meter produced by the Nanjing Soil Instrument Co., Ltd. (Figure 6). This research mainly concerned the impact of different numbers of cycles on soil strength, which could be somewhat biased by the consolidation. Considering the state of soil in practice, we performed rapid shear tests under unconsolidated and undrained (UU) conditions. Based on geotechnical test method standards, the rate of shear strain was selected as 0.6 mm/min (0.5~1.0%/min), and the values of confining pressure were selected as 100, 200, and 300 kPa.

Figure 6. TFB-1 type unsaturated soil stress and strain control-type triaxial meter.

3. Results and Analysis

3.1. Stress–Strain Curves

We performed triaxial shear experiments on the soil samples under three (WD, FT, and WD-FT) cycling modes. Taking into consideration the actual condition of the soil, we chose the rapid shear test and set the shear rate to 0.6 mm/min. We analyzed the experimental results and obtained the correlation profiles between primary stress and axial strain (stress–strain curves). Their trends under different cycling modes were roughly the same, regardless of the confining pressure (first increased and then decreased, after reaching their peak values).

3.1.1. Stress–Strain Curves after WD Cycling

As shown in Figure 7, the principal stress differences of the soil samples were maximized after zero WD cycles; as the frequency of cycles increased, they decreased by different extents. After five and ten WD cycles, the soil samples showed a slight increase in peak principal stress variance because, at this time, a new stable state was reached by the soil. After 15 WD cycles, the peak principal stress difference showed a decreasing trend and tended to be stable.

3.1.2. Stress–Strain Curves after FT Cycling

As shown in Figure 8, under UU conditions, the soil strength first rises, then falls, and stabilizes after FT cycling. The strength degradation intensity of the soil samples was the most pronounced after the first FT cycle. As the test progressed, the strength degradation rate gradually decreased and then stabilized.

3.1.3. Stress–Strain Curves after Coupled WD-FT Cycling

As illustrated in Figure 9, under UU conditions, the highest position of the curve is found under uncoupled WD-FT cycling, and the curve after coupled WD-FT cycling tends to decrease and then stabilize, and the coefficient of variation is greatest in the early stages of the coupled WD-FT cycling. As the number of coupled WD-FT cycles increased, the peak principal stress differences of the soil samples decreased, demonstrating that an increase in the number of coupled WD-FT cycles changed the soil structure, which, in turn, produced soil degradation.

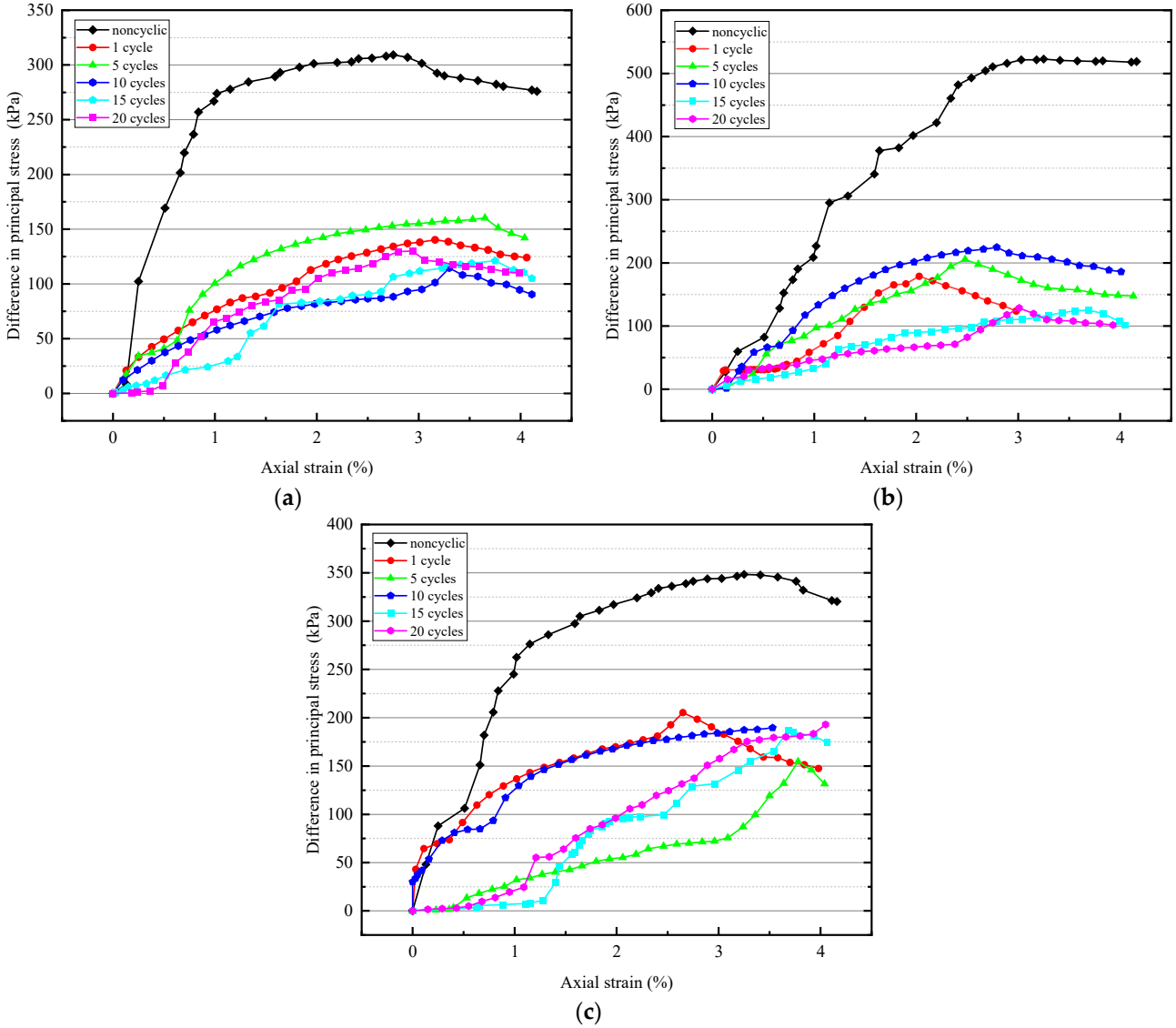

Figure 7. Stress–strain curves under wet and dry cycles: (**a**) Stress curve corresponding to 100 kPa; (**b**) stress curve corresponding to 200 kPa; (**c**) stress curve corresponding to 300 kPa.

3.2. Soil Cohesion and Internal Angle Evolution

3.2.1. Soil Cohesion and Internal Angle Evolution after WD Cycling

For the data acquired in indoor triaxial shearing tests, we performed an analysis of the test data using the Mohr–Coulomb theoretical equations. The shear strength values of loess in the Yili region, i.e., τ, after different numbers of WD cycles were derived as follows, the detailed calculation process can be found elsewhere [29]:

$$\tau = c + \sigma \tan \varphi \quad (1)$$

where c is the soil cohesion, σ is the confining stress, and φ is the internal friction angle.

According to the Mohr–Coulomb stress circle, we obtain:

$$\sin \varphi = \frac{\frac{\sigma_1 - \sigma_3}{2}}{c \cot \varphi + \frac{\sigma_1 + \sigma_3}{2}} \quad (2)$$

where σ_1 and σ_3 are the first and third principal stresses, respectively.

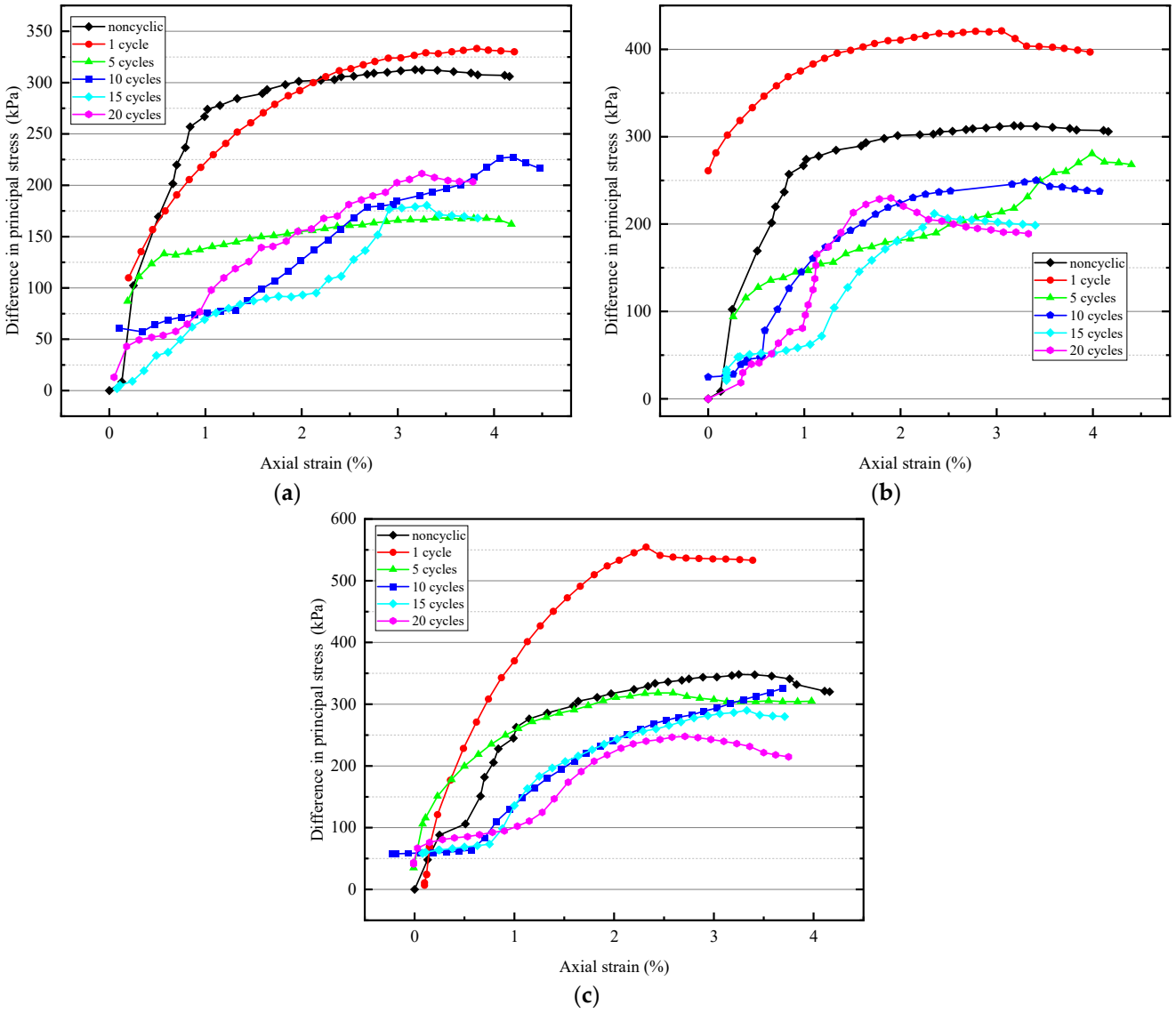

Figure 8. Stress–strain curves under freeze–thaw cycling: (**a**) Stress curve corresponding to 100 kPa; (**b**) stress curve corresponding to 200 kPa; (**c**) stress curve corresponding to 300 kPa.

Re-arrangement of Equation (2) yields:

$$\sigma_1 = A + B\sigma_3, \text{ where } A = \frac{2c\cos\varphi}{1-\sin\varphi} \text{and } B = \frac{1+\sin\varphi}{1-\sin\varphi} \quad (3)$$

The shear strength values of the soil samples after different numbers of WD cycles were calculated using Equation (3) and are listed in Table 1.

Table 1. Shear strength values under wet and dry cycling.

Number of Wet–Dry Cycles	Internal Friction Angle (°)	Cohesion (kPa)
0	25.1768	88.63
1	20.4535	84.32
5	18.8752	85.26
10	20.2371	84.42
15	18.7629	84.82
20	18.3651	85.21

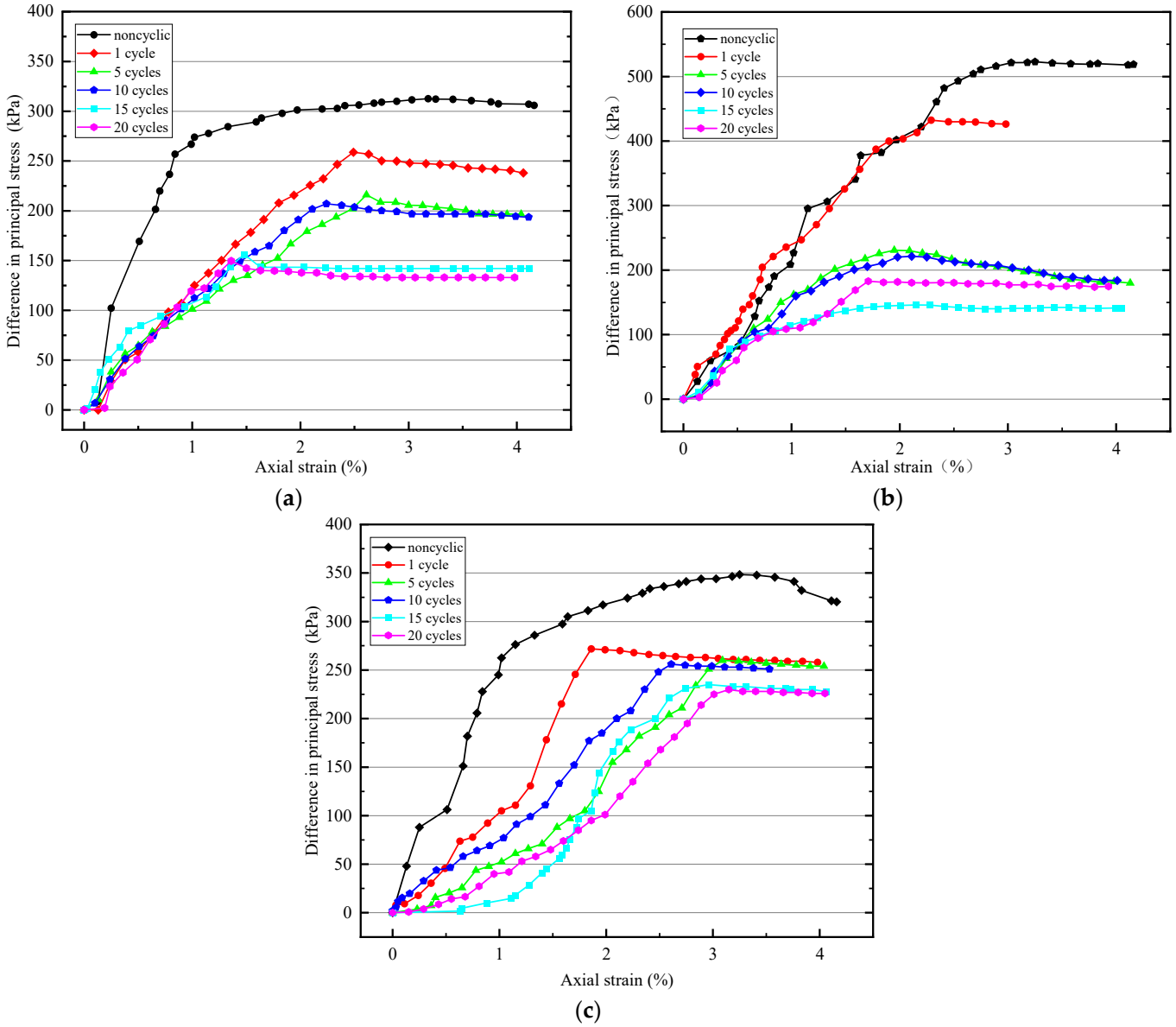

Figure 9. Stress–strain curves under coupled WD-FT cycling: (**a**) Stress curve corresponding to 100 kPa; (**b**) stress curve corresponding to 200 kPa; (**c**) stress curve corresponding to 300 kPa.

As shown in Figure 10, under UU conditions, the angle of internal friction of the soil samples declined with the number of WD cycles. At the first cycle, their slope and decline were the largest; as the test progressed, the internal friction angle gradually tended to be stable, and the final stable value was smaller than the initial value. Soil cohesion decreased significantly after the first WD cycle; as the set test progressed, it fluctuated within a small range (84–88 kPa). Thus, both cohesion and angle of internal friction of the soil decreased with the number of WD cycles, while the former decreased more significantly than the latter.

Hence, the change in soil strength after WD cycling was mainly due to reduced internal friction angle and cohesion.

3.2.2. Soil Cohesion and Internal Angle Evolution after FT Cycling

The shear strength values of the soil samples after different numbers of FT cycles calculated using Equation (3) are listed in Table 2.

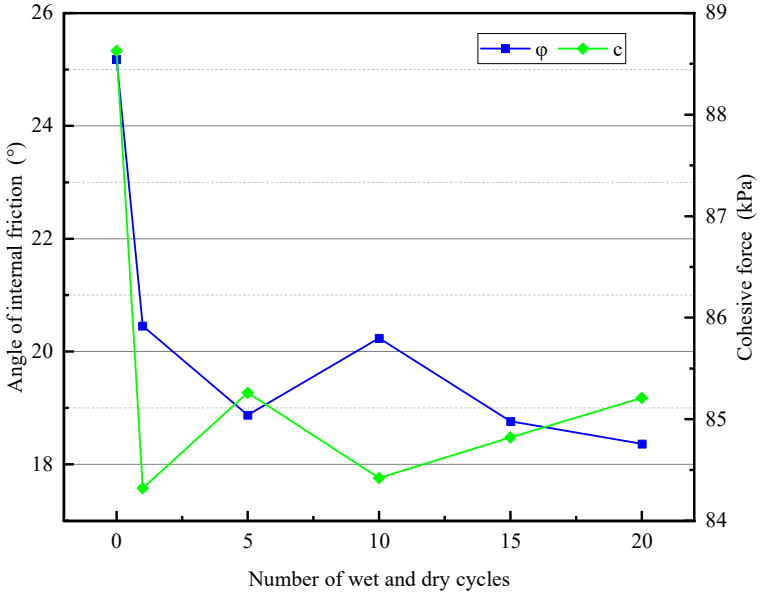

Figure 10. Variations in shear strength with different numbers of wet–dry cycles.

Table 2. Shear strength values under freeze–thaw cycling.

Number of Freeze–Thaw Cycles	Internal Friction Angle (°)	Cohesion (kPa)
0	24.3263	86.77
1	28.2532	85.64
5	22.2441	81.59
10	21.5232	82.65
15	19.8264	82.91
20	19.4024	81.55

As shown in Figure 11, under UU conditions, soil cohesion first decreased, then increased, and eventually stabilized. The inside friction attitude and cohesion confirmed the contrary trend, i.e., they increased first, then decreased, and finally tended to be stable. FT cycles affected each cohesion and inside friction attitude of soil [30]. The combined action of the two led to changes in soil strength.

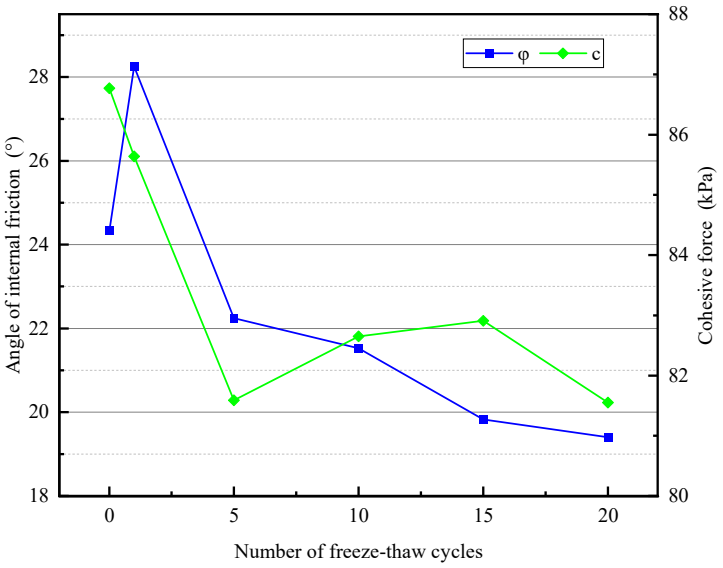

Figure 11. Evolution of shear strength values with different numbers of FT cycles.

3.2.3. Soil Cohesion and Internal Angle Evolution after Coupled WD-FT Cycling

The shear strength values of the soil specimens after different numbers of coupled WD-FT cycles were calculated according to Equation (3) and are summarized in Table 3.

Table 3. Shear strength values under different numbers of coupled WD-FT cycles.

Number of coupled WD-FT Cycles	Internal Friction angle (°)	Cohesion (kPa)
0	24.3263	86.77
1	25.1505	84.64
5	21.3461	82.59
10	18.5262	79.65
15	17.8164	79.91
20	17.4135	78.7

As shown in Figure 12, under UU conditions, soil cohesion decreased first, and then gradually tended to be stable. The inner friction perspective first increased, then decreased, and finally tended to be stable, demonstrating that coupled WD-FT cycling impacted each cohesion and interior friction perspective of soil, resulting in changes in soil strength.

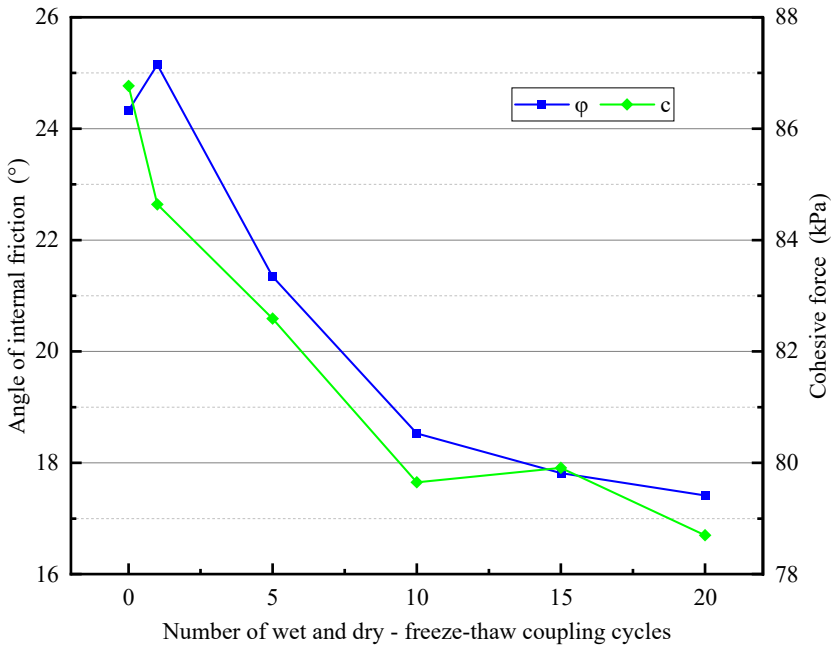

Figure 12. Variation of shear strength values with different numbers of coupled WD-FT cycles.

3.3. Shear Stress Evolution

3.3.1. Shear Stress Evolution with WD Cycling

The shear stress values of the soil samples were calculated using Equation (1) and are listed in Table 4. Figure 13 shows the shear stress curves after WD cycling. As shown in Figure 13, under UU conditions, the shear stress of soil decreased as the number of WD cycles increased and tended to be stable with fluctuations in a small range (5–10 kPa), and the final stable shear stress was lower than the initial shear stress.

Table 4. Shear stress under different numbers of WD cycles.

Number of WD Cycles	σ_3 = 100 kPa	σ_3 = 200 kPa	σ_3 = 300 kPa
0	130.78	177.79	224.8
1	112.93	150.22	187.51
5	118.78	152.97	187.16
10	119.52	156.39	193.26
15	119.88	153.85	187.82
20	117.74	150.93	184.12

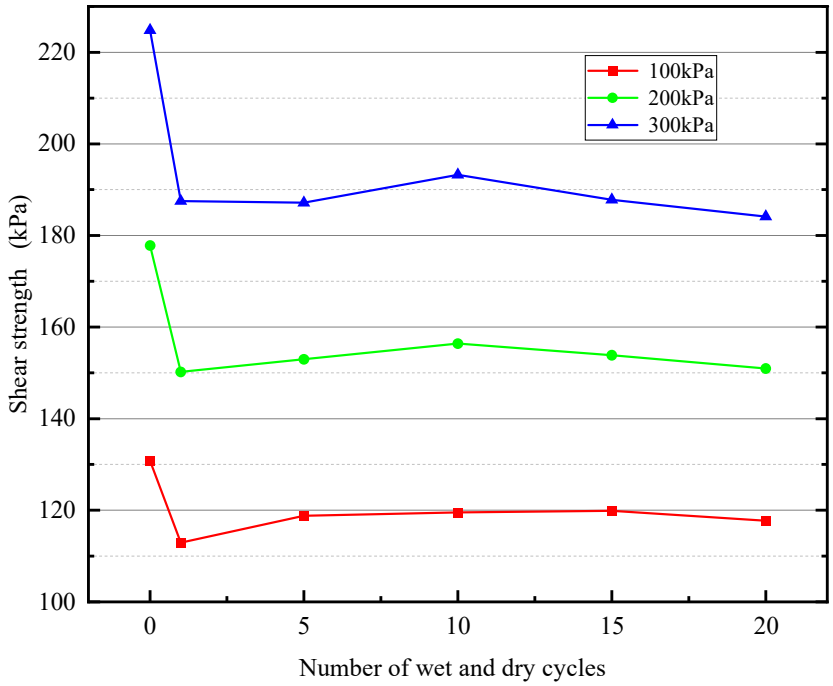

Figure 13. Change in shear stress under WD cycling.

3.3.2. Shear Stress Evolution with FT Cycling

According to the processed experimental data, we adopted Equation (1) and obtained the soil shear stress values; the final outcomes are shown in Table 5. The shear stress curves under FT cycling conditions are shown in Figure 14. As observed, under UU conditions, compared with the soil samples in the initial state, there was a transient increase in strength when undergoing the first FT cycle. As the test progressed, first, it fluctuated within a small range, and then tended to be stable, and the shear stress after stabilization was smaller than that in the initial state.

Table 5. Shear stress under FT cycles.

Number of FT Cycles	σ_3 = 100 kPa	σ_3 = 200 kPa	σ_3 = 300 kPa
0	130.78	177.79	197.81
1	150.92	190.35	207.38
5	134.78	172.42	187.24
10	128.36	166.67	190.75
15	125.46	163.83	189.58
20	127.52	160.62	187.37

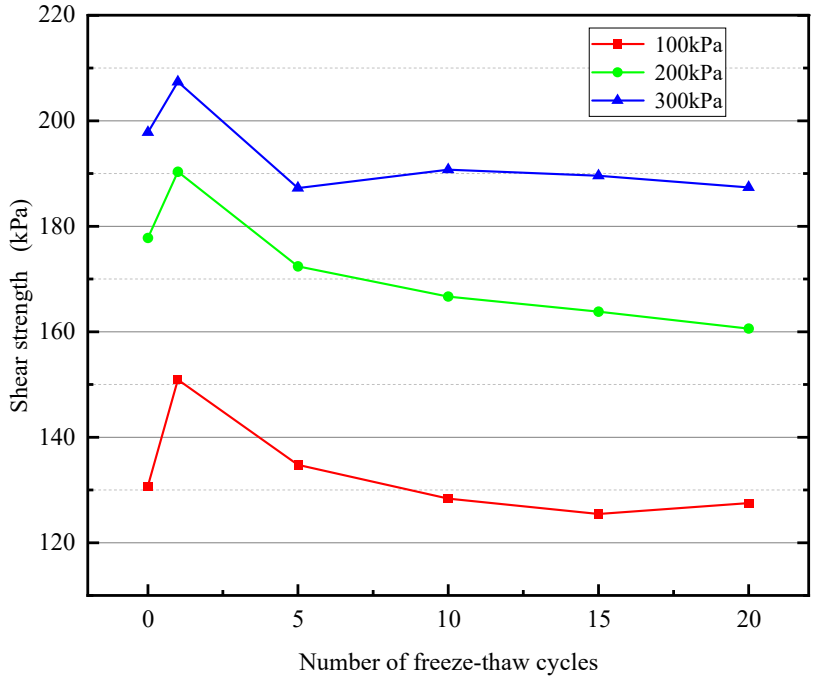

Figure 14. Variations in shear stress under FT cycling.

3.3.3. Shear Stress Evolution with Coupled WD-FT Cycling

According to the calculated cohesion and internal angle values (c and φ), the Mohr–Coulomb regulation and Equation (1) were used to calculate soil shear stress. The calculation results are listed in Table 6. Figure 15 shows the curves of shear stress evolution after different numbers of coupled WD-FT cycles. The soil samples' shear strength gradually decreased and then stabilized, demonstrating that coupled WD-FT cycling had a greater impact on soil shear stress in the early stage. The shear stress of the soil samples showed very little fluctuation as the coupled WD-FT cycles increased, and it stabilized after experiencing fluctuations; the shear stress after stabilization was smaller than that in the initial state of coupled WD-FT cycling.

Table 6. Shear stress values under different numbers of coupled WD-FT cycles.

Number of Coupled Cycles	σ_3 = 100 kPa	σ_3 = 200 kPa	σ_3 = 300 kPa
0	130.78	177.79	197.81
1	125.92	165.35	187.38
5	121.78	160.42	183.24
10	118.36	158.67	179.75
15	117.46	157.83	175.58
20	117.52	157.62	175.37

3.4. Shear Strength Attenuation Mechanisms

3.4.1. Shear Strength Attenuation Mechanism of WD Cycling

(1) Attenuation

The reduction in shear strength, described as the shear strength attenuation (T_τ), after a sure range of WD cycles was calculated using Equation (4):

$$T_{\tau i} = \frac{\tau_{i-1} - \tau_i}{\tau_{i-1}} \times 100\% \quad (4)$$

The calculation results are listed in Table 7.

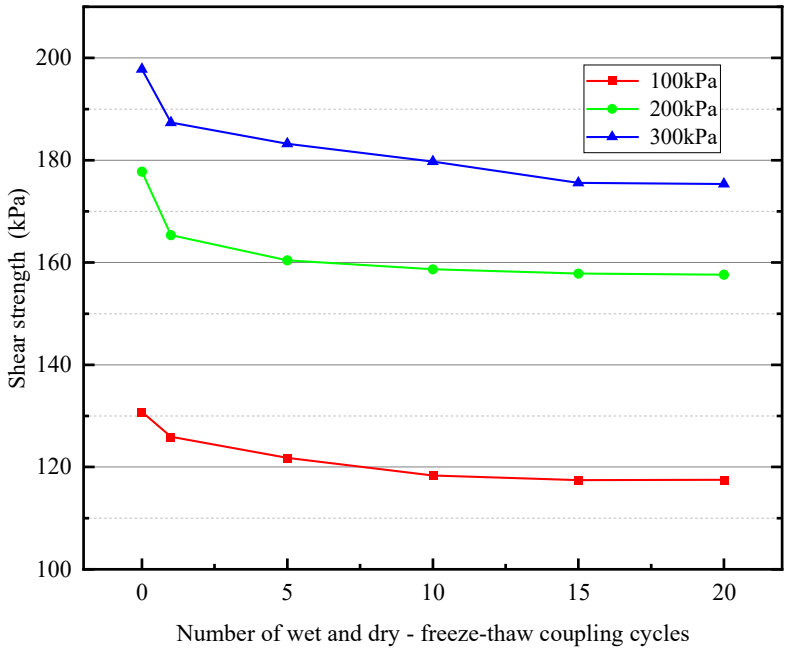

Figure 15. Trend plot of shear stress under the influence of coupled WD-FT cycling.

Table 7. Reduction in shear strength under wet–dry cycling.

Number of Wet and Dry Cycles	σ_3 = 100 kPa	σ_3 = 200 kPa	σ_3 = 300 kPa
0	0	0	0
1	25.56	22.35	37.81
5	0 (−12.41)	0 (−6.77)	0 (−7.98)
10	9.47	12.56	17.42
15	0 (−8.54)	11.32	18.44
20	0 (−3.71)	0 (−13.84)	0 (−7.14)

(2) Attenuation mechanism of WD cycling

After sorting the data in Table 8, we obtained the accumulative attenuation of the shear strength after different numbers of cycles at different confining pressures. As shown in Figure 16, compared with the soil samples in the preliminary state, after one WD cycle, the curve slope and shear strength attenuation were the largest; then, the attenuation curve slope gradually decreased and stabilized.

Table 8. Decrease in shear strength under freeze–thaw cycling.

Number of Freeze–Thaw Cycles	σ_3 = 100 kPa	σ_3 = 200 kPa	σ_3 = 300 kPa
0	0	0	0
1	0 (−15.26)	0 (−12.41)	0 (−24.31)
5	10.41	7.82	6.54
10	0 (−5.46)	1.52	2.37
15	0 (−4.74)	1.39	1.49
20	3.51	0.88	0.24

During the continuous humidification and dehumidification of soil samples in WD cycling, the internal particles underwent a cycle state of water absorption expansion-water loss contraction. In this state, some of the hydrophilic minerals between the soil particles departed from the status quo, decreasing the binding forces between the soil particles and reducing the soil cohesion to a certain extent. Because of continuous soaking and drying, large particles decomposed, and small particles aggregated, resulting in a relative increase

in the range of medium pores and a relative reduction in the quantity of large and small pores. During this process, the soil particles became more rounded, reducing the friction contact forces between the particles and decreasing angle of internal friction. Finally, the soil shear strength gradually decreased after WD cycling, as shown in Figure 17.

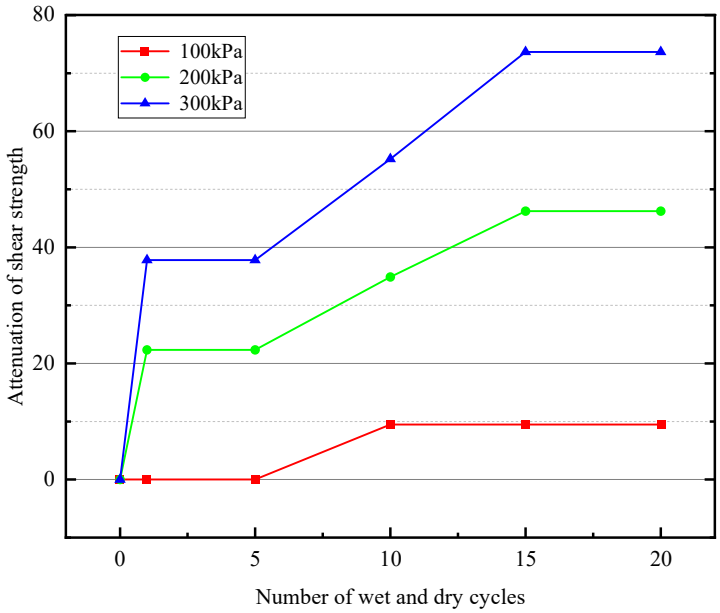

Figure 16. Reduction in shear strength under wet–dry cycling.

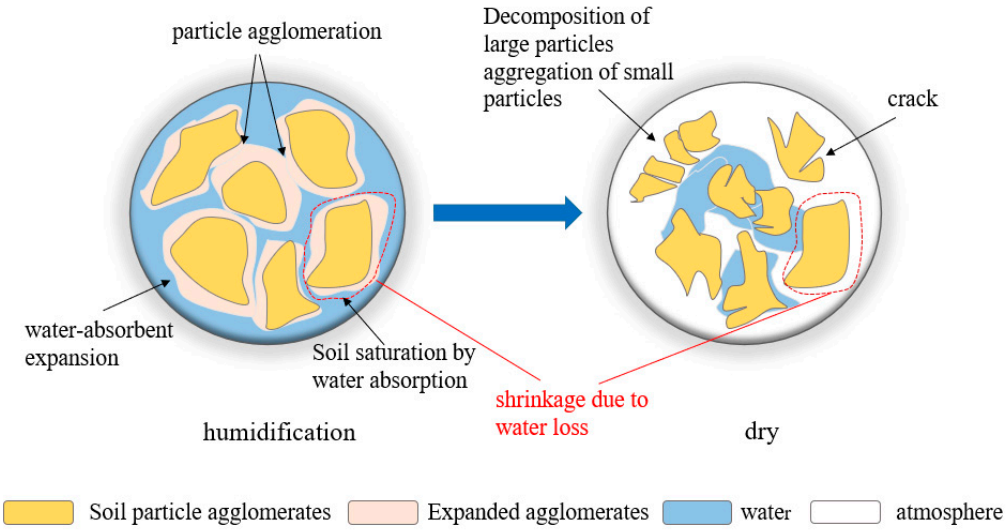

Figure 17. Schematic diagram of soil evolution in wet–dry cycling.

3.4.2. Shear Strength Attenuation Mechanism during FT Cycling

(1) Attenuation

The shear strength decay values of soil samples following FT cycling calculated by Equation (4) are shown in Table 8.

(2) Attenuation mechanism of FT cycling

After sorting the data in Table 9, we obtained the accumulative attenuation of the shear strength after different numbers of FT cycles under confining pressures (see Figure 18). As observed, compared with the soil samples in the initial state, the soil shear strength did not decay after the first cycle; after five FT cycles, shear strength attenuation was the maximum; then, the attenuation curve slope decreased, the change decreased, and finally stabilized.

Table 9. Reduction in shear strength under coupling cycles.

Number of Coupling Cycles	σ_3 = 100 kPa	σ_3 = 200 kPa	σ_3 = 300 kPa
0	0	0	0
1	34.17	33.46	36.72
5	20.42	37.82	38.54
10	0 (−3.46)	22.52	23.37
15	0 (−2.74)	23.39	22.49
20	2.51	0 (−0.88)	0 (−5.74)

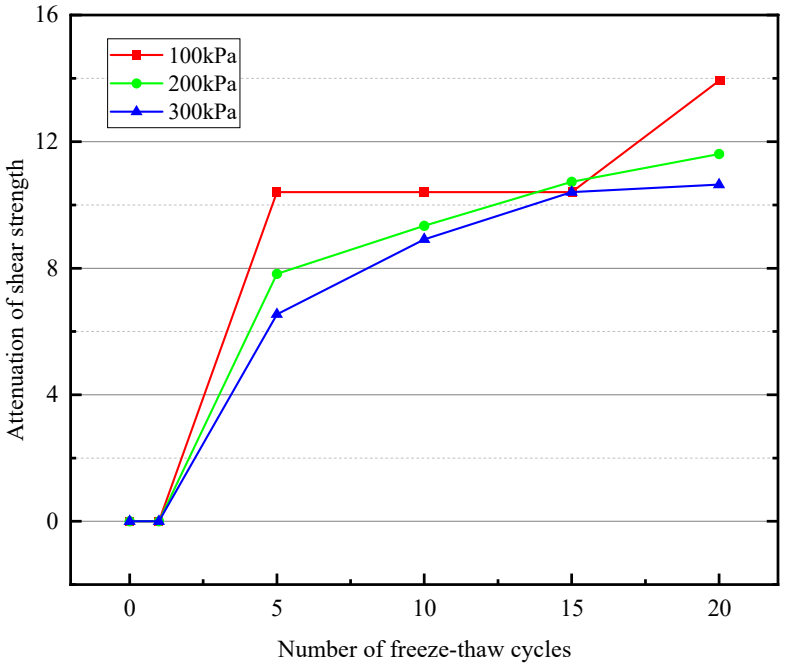

Figure 18. Reduction in shear strength by the action of FT cycles.

After the first freeze–thaw cycle, the shear strength of the soil increases. Because the FT cycle destroys the raw bindings of soil particles, the frost heaving and migration forces generated by water in the soil continuously weakens the adhesion between soil particles, leading to reduced cohesion. Rearrangement of soil particles during migration increases the contact points between particles and increases the angle of internal friction; the two phenomena promote and influence each other, leading to an increase in the soil shear strength.

As more cycles are added, due to the continuous ebb and flow and melting of frost, soil-free water is constantly moving, the binding force between soil particles is reduced, and this process is irreversible, decreasing soil cohesion. Meanwhile, large particles are broken during the migration of soil particles, and small particles aggregate so that the quantity of medium pores increases and those of pores of all sizes decreases. With an increasing number of cycles, the degree of rounding of soil particles continuously increases during this process. There is a gradual decrease in contact points between particles, reducing friction between particles so that the internal friction angle decreases, which eventually leads to a decline in soil shear strength after FT cycling. A schematic diagram of the FT cycle evolution of the soil is shown in Figure 19.

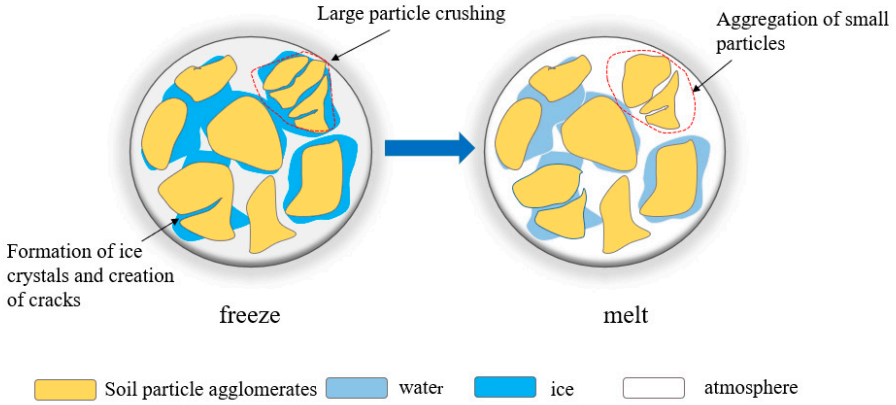

Figure 19. Schematic diagram of soil freeze–thaw cycle evolution.

3.4.3. Attenuation Mechanism of Shear Strength during Coupled WD-FT Cycling

(1) Attenuation

The shear strength decay values of soil samples following WD-FT cycling calculated by Equation (4) are shown in Table 9.

(2) Attenuation mechanism of WD-FT cycling

Figure 20 shows the accumulative attenuation of shear strength under different numbers of coupled WD-FT cycles and different confining pressures.

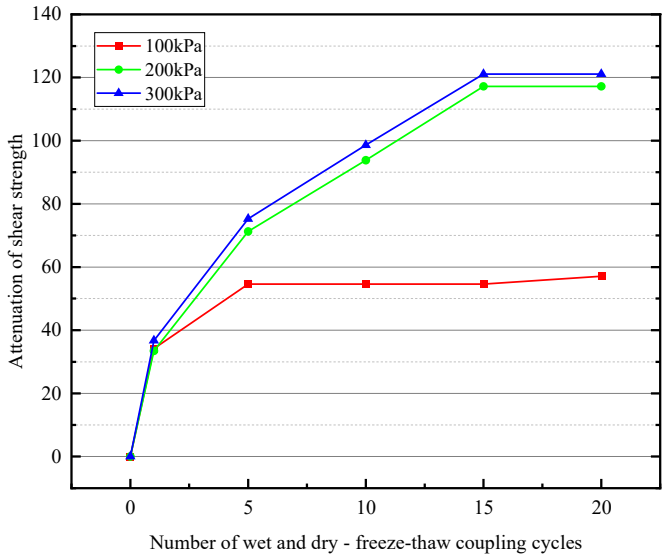

Figure 20. Shear strength reduction under coupled cyclic action.

As observed, shear strength attenuation improved, and then stabilized as the number of coupled WD-FT cycles increased. After one WD-FT coupling cycle, the soil shear strength had the largest attenuation curve slope because the coupled WD-FT cycling made its internal particles undergo the processes of imbibition (water absorption), dehydration, freezing, and melting. During the process of imbibition and water loss, the binding between soil particles gradually decreased so that the original cementation between soil particles was destroyed, and this process was irreversible. At the same time, the large- and middle-sized particles were crushed, increasing the share of large and small particles, and decreasing the angle of internal friction. Subsequently, during the FT processes, the frost heave and migration forces generated through the water in the soil due to freezing and migration continuously weakened the cohesion between soil particles, and resulting in a reduction in cohesion. The soil particles rearranged during the migration process, and the contact

points between the particles increased, resulting in a temporary increase in the interior friction angle. After many coupled WD-FT cycles, the inherent cementation between soil particles was repeatedly destroyed by the constant processes of infiltration, water loss, freezing, and thawing. However, during the redistribution of particles within, new contact and cementation points were formed; after 15 coupled WD-FT cycles, the soil shear strength stabilized, demonstrating that a new stable state was formed, but overall, the values were smaller than those before coupled cycling. This implied that coupled WD-FT cycling decreased the inside friction angle and cohesion of soil, and the former's reduction exceeded the latter's, eventually deteriorating the soil shear strength, as illustrated in Figure 21.

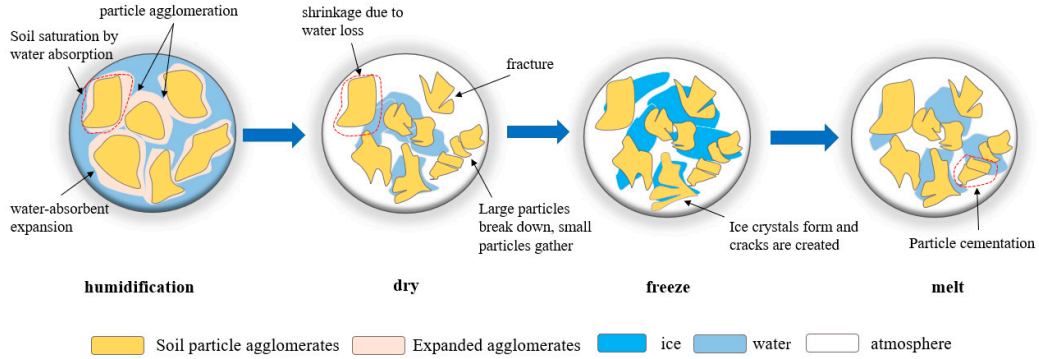

Figure 21. Schematic diagram of the evolutionary mechanism of coupled WD-FT cycling in soil.

4. Discussion

4.1. Shear Strength Evolution and Attenuation Trends

We processed the indoor triaxial shear test data to obtain the change in shear strength attenuation (see Figure 22) and compared the test results obtained under the three cycling modes. Figure 22a compares the internal friction angles of soil samples after WD, FT, and coupled WD-FT cycling. Figure 22b compares the cohesion changes after WD, FT, and coupled WD-FT cycling. Figure 22c–e illustrate shear strength attenuation under different confining pressures after WD, FT, and coupled WD-FT cycling.

During WD cycling, the water content of soil changed from natural to saturated, changing the status of effective pores in the soil from partially filled with water to fully filled. At this time, part of the hydrophilic minerals in the soil broke away from the original state, destroying the original cementation and violating the original consolidation state. It changed the soil skeleton and promoted an increase in the medium pore content, and the process was irreversible. However, during FT cycling, there was no change in moisture content. As the freezing action proceeded, the soil gradually froze from the outside to the inside, and during this process, the internal free water began to migrate to the freezing front and ice accumulation on the soil surface gradually increased. At the same time, freezing and migration forces due to freezing and migration of water in soils continuously reduced the occlusal force of soil particles and the original consolidation effect. During the melting process, the internal ice turned into water, and the fluidity of the water promoted the migration of some soil particles. During the migration process, the position of particles and soil skeleton changed.

WD and FT cycling affected the bonding of soil particles to each other. On the one hand, WD cycling led to crack propagation, resulting in broken particle connections. On the other hand, FT cycling filled fine-grained sticky soil particles, resulting in weakened interparticle cementation. The impact of coupled WD-FT cycling on soil cohesion was determined by the superposition effect of the two. Therefore, the degree of soil damage and cohesion decreased the most in coupled WD-FT cycling [31,32].

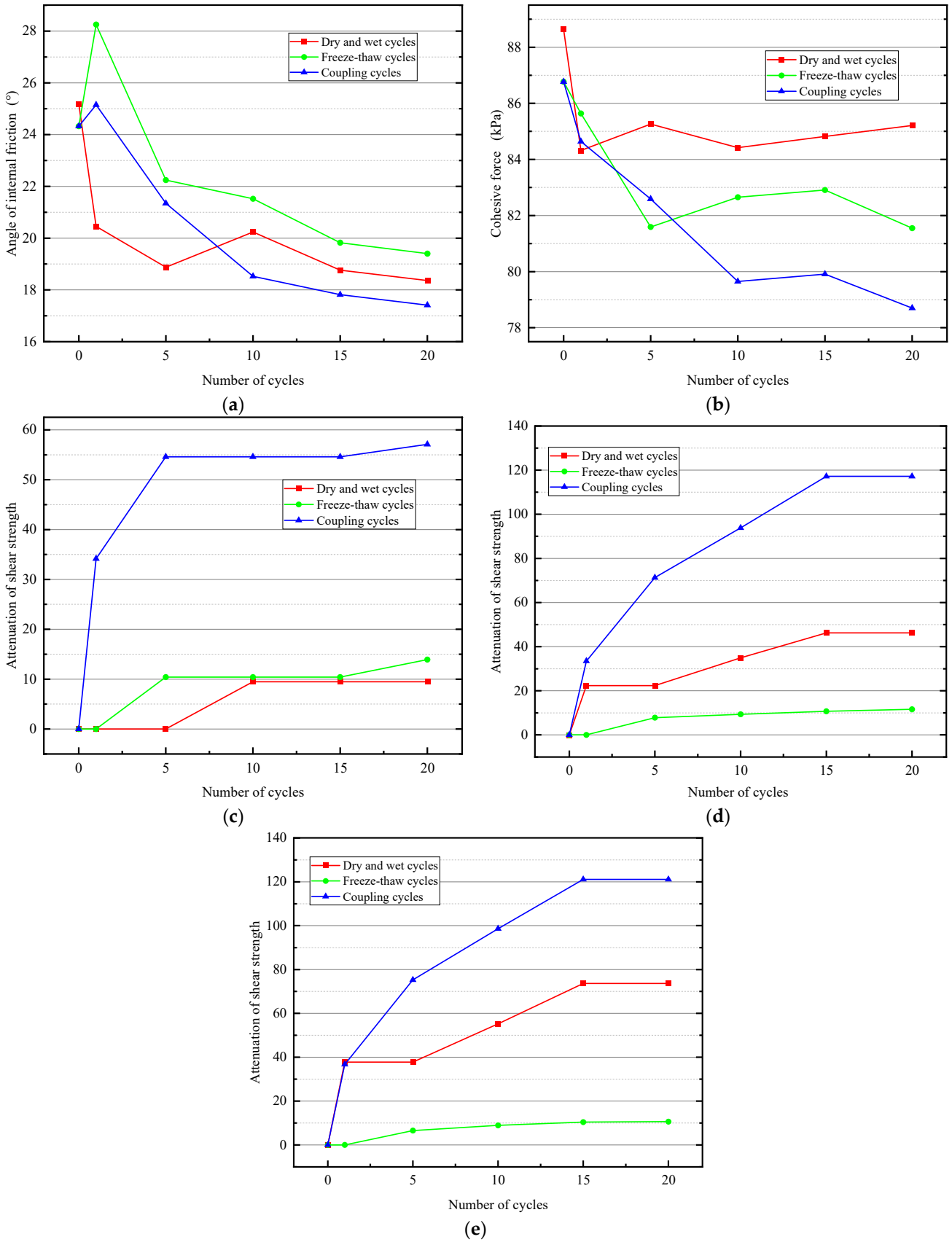

Figure 22. Comparison of three cycling conditions. (**a**) Change in angle of internal friction; (**b**) Change in cohesion; (**c**) 100 kPa; (**d**) 200 kPa; (**e**) 300 kPa.

As shown in Figure 22, the impact of coupled WD-FT cycling on soil strength was the most significant, observed by way of WD cycling, while FT cycling had the least impact. The best effect of all three occurred at the time of the first cycle, i.e., the first wet–dry, freeze–thaw, and coupled wet–dry and freeze–thaw cycles had the greatest effect on the mechanical characteristics of the soils. From the angle of internal friction, cohesion, and shear strength attenuation, the effect of coupled WD-FT cycling on soil shear strength is not a simple one-factor additive–subtractive arithmetic relationship; it exceeds the effect of a single (WD or FT) factor, but is less than the sum of them. This was mainly due to the different shares of wet–dry and freeze–thaw cycles in coupled WD-FT cycling, and the combined effect of the two led to changes in soil strength.

4.2. Weight Analysis of Each Single Factor's Contribution in Coupled WD-FT Cycling

As mentioned above, in the coupled WD-FT cycling, WD and FT cycles affected the soil shear strength not independently but were coupled. This study analyzed the respective contributions (weights) of WD and FT cycles to the soil strength degradation.

We analyzed the three-dimensional scatter plots (Figure 23) drawn with the independent and dependent variables. As observed, the relationships among the three variables were roughly linear, so we used multivariate linear regression to analyze them. Multivariate linear regression is commonly used to analyze the correlations between multiple independent and dependent variables. At the same time, it can also obtain the energy efficiency of different independent variables on dependent variables [33]. In this paper, independent variables were shear strength decay values during wet–dry and during freeze–thaw cycling, and the dependent variable was shear strength decay during coupled WD-FT cycling. A multivariate regression model was established as follows:

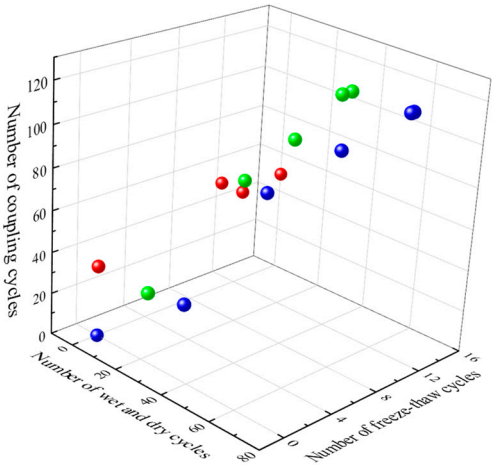

Figure 23. Three-dimensional scatter plot.

We assumed a linear regression relationship between the dependent variable y and the independent variables $x_1, x_2, \ldots, x_n$ for their ith data [34]:

$$(yi,\ xi1,\ xi2,\ \ldots,\ xik),\ i = 1,\ 2,\ 3\ldots,\ n, \tag{5}$$

Hence,

$$\begin{cases} = \beta 0 + \beta 1x11 + \beta 2x12 + \ldots + \beta kx1k + \varepsilon 1 \\ = \beta 0 + \beta 2x21 + \beta 2x22 + \ldots + \beta kx2k + \varepsilon 2 \\ \qquad\qquad \ldots \\ = \beta 0 + \beta 1xn1 + \beta 2xn2 + \ldots + \beta kxnk + \varepsilon n \end{cases} \tag{6}$$

where β_0, β_1, …, β_k are $k + 1$ unknown parameters, and x_1, x_2, …, x_{1k} are k controllable variables, then:

$$\begin{bmatrix} y_1 \\ y_2 \\ \cdots \\ y_n \end{bmatrix} = \begin{bmatrix} 1 & x_{11} & x_{12} & \cdots & x_{1k} \\ 1 & x_{21} & x_{22} & \cdots & x_{2k} \\ \cdots & \cdots & \cdots & \cdots & \cdots \\ 1 & x_{n1} & x_{n2} & \cdots & x_{nk} \end{bmatrix} \begin{bmatrix} \beta_0 \\ \beta_1 \\ \cdots \\ \beta_k \end{bmatrix} + \begin{bmatrix} \varepsilon_1 \\ \varepsilon_2 \\ \cdots \\ \varepsilon_n \end{bmatrix} \quad (7)$$

Hence, the multivariate regression model is as follows:

$$\begin{cases} X\beta + \varepsilon \\ \varepsilon \sim Nn\left(0,\ \sigma^2 In\right) \end{cases} \quad (8)$$

where X is a full-rank matrix, $E\varepsilon = 0$ is an n-dimensional 0 vector, and I_n is an n-order identity matrix.

The SPSS statistical software (IBM SPSS Statistics 25) was used for multivariate regression analysis in this paper. We set the shear strength attenuation obtained after WD cycling as x_1, the shear strength attenuation obtained after FT cycling as x_2, and the shear strength attenuation obtained after coupled WD-FT cycling as y. Then, we obtained the multivariate regression model between the dependent and independent variables, as shown in Table 10.

Table 10. ANOVA table for the regression model.

Model	Square Sum	Degrees of Freedom	Mean Square	F	Significance
Total regression residuals	275.12	2	95.32	355.71	0.000
	21.42	107	0.23		
	301.61	112			

As shown in Table 10, when testing the regression model, the F statistic was 355.71 and the significance probability was $p = 0.000$, which was less than $\alpha = 0.001$, so the developed regression model was significant.

As indicated in Table 11, when testing the shear strength attenuation of soil after WD cycling, the t-test statistic was 6.42. The probability of significance was $p = 0.000$, less than $\alpha = 0.001$, suggesting that the impact of soil after WD cycling on the shear strength attenuation of soil after coupled WD-FT cycling was significant. When testing the shear strength attenuation of soil after FT cycling, the t-test statistic was 6.48, and the probability of significance was $p = 0.000$, less than $\alpha = 0.001$, suggesting that the effect of the shear strength attenuation of soil after FT cycling on the shear strength attenuation of soil after coupled WD-FT cycling was significant. Likewise, under coupled WD-FT cycling, the number of cycles had a significant effect on soil shear strength attenuation. Therefore, the regression model was established in the following form:

$$\hat{y} = 0.55 + 0.33x_1 + 0.57x_2 + 0.01n \quad (9)$$

Table 11. Table of regression model coefficients.

Model		Unstandardized Coefficient		Standardized Coefficient	t	Significance
		B	Standard Error	Beta		
Variant	(Constant)	0.53	0.07		6.31	0.000
	Dry–wet cycle	0.32	0.06	0.42	6.42	0.000
	Freeze–thaw cycle	0.52	0.08	0.61	6.48	0.000
	Number of cycles	0.01	0.00	0.03	4.32	0.000

We performed a linear regression analysis on different variables and found that WD cycling had the greatest impact on shear strength attenuation, with a weight of 0.57; FT

cycling had the second greatest influence on the shear strength attenuation of soil samples under coupled WD-FT cycling, with a weight of approximately 0.33; and the total number of cycles had a slight effect on the final result, with a weight of 0.01. It can be considered that the number of cycles did not affect the shear strength attenuation of soil samples.

5. Conclusions

This study investigated loess samples collected in a typical loess landslide, i.e., the Alemale landslide slip zone soil in the Yili region, China. Triaxial shear tests of soil samples after WD, FT, and coupled WD-FT cycling were carried out to discover the evolution of their mechanical performances in different cycling modes and to reveal the corresponding degradation mechanisms of loess in the Yili region. Based on the outcomes obtained, the conclusions below are drawn:

(1) Under different cycling modes, the tendency of changes in principal stresses of soil samples is basically the same (increasing, reaching a peak, and then gradually decreasing and stabilizing), independent of the confining pressure.
(2) Under UU conditions, the soil samples' internal friction angle and cohesion values had varying degrees of decline after WD cycling. Both parameters changed the most during the first WD cycle, and as the number of cycles increased, their variation range decreased and gradually stabilized. After FT cycling, the internal friction angle of the soil samples first increased, then decreased, and finally stabilized, while the soil cohesion first decreased and then stabilized. As the number of coupled WD-FT cycles increased, the loess cohesion first decreased and then gradually stabilized, while the internal friction perspective improved first, then reduced, and eventually it gradually stabilized, demonstrating that coupled WD-FT cycling had an impact on both the cohesion and internal friction angle of soil, resulting in changes in soil strength.
(3) The soil shear strength of the soil samples decreased after 20 cycles under all cycling modes, while the trends were different. Herein, the soil shear strength of samples decreased drastically after WD cycling and stabilized after small fluctuations; after FT cycling, the soil shear strength of samples increased, then decreased, and stabilized after fluctuations; as the number of coupled WD-FT cycles increased, the soil shear strength decreased first, and then stabilized.
(4) The regression model based on the weight analysis of each single factor in coupled WD-FT cycling and the linear regression analysis of different variables revealed that the weights (contributions) of the impacts of WD cycling, FT cycling, and the total number of cycles on shear strength attenuation of soil samples were 0.57, 0.33, and 0.01, respectively.

Author Contributions: Conceptualization, Y.Z. (Yongliang Zhang); Methodology, W.H.; Software, Y.Z. (Yongliang Zhang) and Y.W.; Validation, Y.Z. (Yongliang Zhang) and Y.W.; Formal analysis, Y.Z. (Yongliang Zhang), W.H. and Y.Z. (Yanyang Zhang); Investigation, Y.Z. (Yongliang Zhang), Y.Z. (Yanyang Zhang) and G.S.; Resources, Z.Z. and G.S.; Data curation, Z.Z. and W.H.; Writing—original draft, Y.Z. (Yongliang Zhang); Writing—review & editing, Y.Z. (Yongliang Zhang), Z.Z. and W.H.; Visualization, Z.Z., Y.Z. (Yanyang Zhang), G.S. and Y.W.; Supervision, Z.Z., Y.Z. (Yanyang Zhang) and G.S.; Project administration, Z.Z.; Funding acquisition, Z.Z. All authors have read and agreed to the published version of the manuscript.

Funding: This research was funded by The National Natural Science Foundation of China, grant number 41967036, and Xinjiang Uygur Autonomous Region Special Program for Key R&D Tasks, grant number 2021B03004.

Data Availability Statement: Not applicable.

Conflicts of Interest: The authors declare no conflict of interest.

References

1. Song, Y.; Zhu, P.; Lu, T.; Qi, C. Experimental Study of Wetting-Drying Cycle on Deformation Behaviors of Unsaturated Remoulded Clay. *Chin. J. Undergr. Space Eng.* **2022**, *18*, 1219–1225+1240.
2. Yu, L.E.I.; Aihua, L.; Mingjiang, D. Analyses of the climate change and its impact on water resources in the middle reaches of Irtysh River during 1926–2009. *J. Glaciol. Geocryol.* **2012**, *34*, 912–919.
3. Zhao, X. Investigation on the Influence of Freezing-Thawing Cycle and Drying-Wetting Alternation on the Permeability Anisotropy and Spatial Variability of Loess. Master's Thesis, Xi'an University of Architecture and Technology, Xi'an, China, 2019. (In Chinese)
4. Li, G.; Wang, F.; Ma, W.; Fortier, R.; Mu, Y.; Mao, Y.; Hou, X. Variations in strength and deformation of compacted loess exposed to wetting-drying and freeze-thaw cycles. *Cold Reg. Sci. Technol.* **2018**, *151*, 159–167. [CrossRef]
5. Zhou, Z.; Ma, W.; Zhang, S.; Mu, Y.; Li, G. Effect of freeze-thaw cycles in mechanical behaviors of frozen loess. *Cold Reg. Sci. Technol.* **2018**, *146*, 9–18. [CrossRef]
6. Zhu, J.; Han, S.; Zhang, H. Compression behavior and structure of undisturbed Q2 loess under wet-dry cycles. *Soils Found.* **2022**, *62*, 101165. [CrossRef]
7. Ni, W.K.; Yuan, K.Z.; Lü, X.F.; Yuan, Z.H. Comparison and quantitative analysis of microstructure parameters between original loess and remoulded loess under different wetting-drying cycles. *Sci. Rep.* **2020**, *10*, 5547. [CrossRef]
8. Wu, H.; Shao, S.; Shao, S.; Zhang, S.; Wang, Z. Variations in dynamic shear modulus of loess exposed to dry-wet cycles from Xi'an area, China. *Soil Dyn. Earthq. Eng.* **2023**, *173*, 108126. [CrossRef]
9. Lian, B.; Wang, X.; Zhan, H.; Wang, J.; Peng, J.; Gu, T.; Zhu, R. Creep mechanical and microstructural insights into the failure mechanism of loess landslides induced by dry-wet cycles in the Heifangtai platform, China. *Eng. Geol.* **2022**, *300*, 106589. [CrossRef]
10. Jing, J.; Hou, J.; Sun, W.; Chen, G.; Ma, Y.; Ji, G. Study on influencing factors of unsaturated loess slope stability under dry-wet cycle conditions. *J. Hydrol.* **2022**, *612*, 128187. [CrossRef]
11. Cai, Z.; Zhu, X.; Huang, Y.; Zhang, C. Influences of freeze-thaw process on evolution characteristics of fissures in expensive soils. *Rock Soil Mech.* **2019**, *40*, 4556–4563.
12. Xu, J.; You, Z.; Sun, F.; Li, Y.; Cheng, J.; Qu, L. Experimental study on the deterioration characteristics of the remolded loess with Na2SO4 under freezing-thawing cycles. *Cold Reg. Sci. Technol.* **2023**, *210*, 103818. [CrossRef]
13. Lu, Z.; Xian, S.; Yao, H.; Fang, R.; She, J. Influence of freeze-thaw cycles in the presence of a supplementary water supply on mechanical properties of compacted soil. *Cold Reg. Sci. Technol.* **2019**, *157*, 42–52. [CrossRef]
14. Ni, W.K.; Shi, H.Q. Influence of freezing-thawing cycles on micro-structure and shear strength of loess. *J. Glaciol. Geocryol.* **2014**, *36*, 922–927.
15. Zhao, G.-T.; Han, Z.; Zou, W.-L.; Wang, X.-Q. Evolution of mechanical behaviours of an expansive soil during drying-wetting, freeze–thaw, and drying-wetting-freeze–thaw cycles. *Bull. Eng. Geol. Environ.* **2021**, *80*, 8109–8121. [CrossRef]
16. Ding, L.Q.; Vanapalli, S.K.; Zou, W.L.; Han, Z.; Wang, X.Q. Freeze-thaw and wetting-drying effects on the hydromechanical behavior of a stabilized expansive soil. *Constr. Build. Mater.* **2021**, *275*, 122162. [CrossRef]
17. Jiang, Q.; Xu, Y.; Wang, H.; Yang, L. Effect of Drying-wetting Cycles on Matric Suction and Shear Strength of Slip Zone Soil. *J. Earth Sci. Environ.* **2022**, *44*, 959–970.
18. Pan, Z.; Yang, G.; Ye, W.; Tian, J.; Liang, B. Study on mechanical properties and microscopic damage of undisturbed loess under dry and wet cycles. *J. Eng. Geol.* **2020**, *28*, 1186–1192.
19. Chang, Z.; Yan, C.; An, N.; Lan, H.; Shi, Y.; Bao, H.; Xu, J. Permeability and Soil Water Characteristic Curve of Undisturbed Loess under Wetting-drying Cycles. *J. Yangtze River Sci. Res. Inst.* 2023. Available online: http://kns.cnki.net/kcms/detail/42.1171.TV.20230118.0919.001.html (accessed on 1 August 2023). (In Chinese).
20. Hao, R.; Zhang, Z.; Guo, Z.; Huang, X.; Lv, Q.; Wang, J.; Liu, T. Investigation of changes to triaxial shear strength parameters and microstructure of yili loess with drying–wetting cycles. *Materials* **2021**, *15*, 255. [CrossRef]
21. Xie, B.; Zhang, W.; Sun, X.; Huang, Y.; Liu, L. Experimental Study on the Effects of Freeze–Thaw Cycles on Strength and Microstructure of Xining Region Loess in China. *Buildings* **2022**, *12*, 795. [CrossRef]
22. Hotineanu, A.; Bouasker, M.; Aldaood, A.; Al-Mukhtar, M. Effect of freeze-thaw cycling on the mechanical properties of lime-stabilized expansive clays. *Cold Reg. Sci. Technol.* **2015**, *119*, 151–157. [CrossRef]
23. Tang, L.; Cong, S.; Geng, L.; Ling, X.; Gan, F. The effect of freeze-thaw cycling on the mechanical properties of expansive soils. *Cold Reg. Sci. Technol.* **2018**, *145*, 197–207. [CrossRef]
24. Wang, D.Y.; Ma, W.; Niu, Y.H.; Chang, X.X.; Wen, Z. Effects of cyclic freezing and thawing on mechanical properties of Qinghai–Tibet clay. *Cold Reg. Sci. Technol.* **2007**, *48*, 34–43. [CrossRef]
25. Lv, Q.; Zhang, Z.; Zhang, T.; Hao, R.; Guo, Z.; Huang, X.; Zhu, J.; Liu, T. The Trend of Permeability of Loess in Yili, China, under Freeze–Thaw Cycles and Its Microscopic Mechanism. *Water* **2021**, *13*, 3257. [CrossRef]
26. Zhang, W. Experimental Study on Compressive Deformation and Microscopic Properties of Remolded Loess under Coupling Effect of Dry-Wet and Freezing-Thawing. Master's Thesis, Chang'an University, Xi'an, China, 2018. (In Chinese).
27. Zhu, R.; Cai, Z.; Huang, Y.; Zhang, C.; Guo, W.; Wang, Y. Effects of wetting-drying-freezing-thawing cycles on mechanical behaviors of expansive soil. *Cold Reg. Sci. Technol.* **2022**, *193*, 103422. [CrossRef]

28. Yang, A.; Wang, B.; Jiang, S. Dynamic characteristics of alkali slag cured lightweight soil under action of dry and wet freezing and thawing. *J. Eng. Geol.* **2022**, *30*, 1962–1973.
29. Heymann, J. *Coulomb's Memoir on Statics*; Cambridge University Press: Cambridge, UK, 1972.
30. Zhao, L.; Peng, J.; Ma, P.; Leng, Y.; Ma, Z. Microstructure response to shear strength deterioration in loess after freeze-thaw cycles. *Eng. Geol.* **2023**, *323*, 107229. [CrossRef]
31. Zhang, L.; Zhang, H.; Cui, Z. Study on mechanical properties and physical mechanism of expansive soil under different cyclic modes. *China Civ. Eng. J.* **2023**, 1–14. (In Chinese) [CrossRef]
32. Zhang, Y.; Zhang, Z.; Hu, W.; Zhang, Y. Evolution and Influencing Mechanisms of the Yili Loess Mechanical Properties under Combined Wetting-Drying and Freeze-Thaw Cycling. *Materials* **2023**, *16*, 4727. [CrossRef]
33. Bai, R.; Xu, X.; Hua, S.; Wang, J. Significant analysis of the influence factors on strength of frozen soil base on multivariable linear regression model. *J. Glaciol. Geocryol.* **2019**, *41*, 416–423.
34. Qian, Z.; Jinxi, Y.; Jinping, Z. Experimental study on permeability of undisturbed loess under freezing-thawing and drying-wetting cycling conditions. *Chin. J. Geol. Hazard Control* **2020**, *31*, 119–126. (In Chinese)